Acc. Chem. Res. **1999,** *32,* 247−255

Surface Analytical Studies of Interface Formation in Organic Light-Emitting Devices

YONGLI GAO

Department of Physics and Astronomy, University of Rochester, Rochester, New York 14627

Received April 1, 1998

1. Introduction

Current research on light-emitting devices using organic materials (OLED) is ultimately aimed at producing an efficient and large-area display device with full color. Recent research has indicated that OLEDs indeed have the necessary attributes and competitive advantages to be considered seriously for display applications.[1] The luminous efficiency is among one of the highest for emissive displays. The discovery of electroluminescence (EL) in poly(*p*-phenylenevinylene) (PPV) by the Cambridge group in 1990 has further attracted interest in this research area and opened up new possibilities.[2] One of the advantages of OLED is the wide tunability of emission wavelength, therefore enabling full color display. Furthermore, it has also been demonstrated that OLEDs can be made flexible[3] or transparent,[4] both difficult to realize by using crystalline inorganic semiconductor materials. The more recent discovery of optically pumped lasing of PPV further stimulated research activities aimed at organic laser diodes.[5]

The current understanding of the devices has been primarily based on macroscopic properties (i.e., work function, electron affinity, ionization potentials, etc.) of the organic layer and the electrodes. However, the interfaces in these devices dictate their performance, and the understanding of the interfaces has a tremendous impact on the device technology. In this Account, I discuss the basic concepts of interface formation in organic semiconductor devices, the methology of probing the interfaces using surface analytical means, and the up-to-date microscopic understanding of the electronic, chemical, and morphological structures of the interfaces.

The OLED device structure generally consists of, in sequence, an indium tin oxide (ITO) covered glass as the anode, a thin layer (multiple layers) of organic materials, and an evaporated metal film as the cathode. Among all organic semiconductor devices, the charge transport process across interfaces of dissimilar materials is of vital importance. The advances in OLEDs are made possible by engineering a thin film device with highly emissive organic materials and excellent interfacial properties for modulating carrier transport and recombination.[1] Transport and EL measurements show that metals of low work function, such as Ca, inject electrons more efficiently than do those of higher work function, giving rise to brighter EL.[6−8] It has also been empirically observed that a thin metal oxide layer between the polymer and the metallic cathode actually improves the performance of the LED device.[9,10] A number of groups have reported that the OLED device performance can be significantly improved if an insulating layer of well-controlled thickness of a few nanometers is inserted between the organic material and the metal cathode.[10−14] It is observed that a single Al layer blocks the Li layer from the organic material and results in a more stable device.[15] Treatment of the ITO surface by depositing a thin carbon layer,[16] by derivatizing with a functionalized oligophenylene layer,[17] by oxygen plasma,[18] or by ink jet printing of a polythiophene layer[19] have also demonstrated improved OLED device performance. One of the device degradation modes of OLEDs has been identified as the formation of black nonemissive spots initialized at the metal/organic interface by dust particles.[20] These observations have demonstrated that understanding and engineering of interfaces are key elements for the future improvement of OLEDs.

2. Theoretical Modeling

The theoretical aspects of interface formation in OLED devices have some resemblance to those of inorganic ones because active materials in both cases are semiconductors. This allows one to use to a certain degree the extensive knowledge accumulated from many years of studies of the electronic properties of inorganic semiconductors. However, the electronic properties of organic materials differ qualitatively from those of crystalline inorganic semiconductors in several important aspects. In crystalline materials, the three-dimensional arrangement of the atoms and their resulting interactions ultimately determine the properties of the materials, but organic molecules and conjugated polymers have to be treated as zero- or quasi one-dimensional entities, respectively.[21] Even for the quasi one-dimensional conjugated polymers, the conformational changes along the chain set limited conjugation lengths. As a result, hopping among the zero-dimensional molecules or the finite conjugated sections of the polymers is the main mechanism of charge transport. Furthermore, the easy deformability of the organic materials results in the formation of polarons, self-trapped charge carriers stabilized by the surrounding structure change. These properties of organic materials demonstrate that many ideas advanced to explain inorganic semiconductors do not directly carry over to organic semiconductors.

2.1. Thermodynamic Model. The thermodynamic model treats organic semiconductors as bulk materials and searches the conditions for thermodynamic equilibrium

Yongli Gao received his B.S. (1981) in physics from Central-South Institute of Mining and Metallurgy, China, and his Ph.D. (1986) in physics from Purdue University under the guidance of Professor Ron Reifenberger. From 1986 to 1988 he was a postdoctoral fellow with Professor John Weaver at the University of Minnesota. Since then, he has been on the faculty of the University of Rochester.

10.1021/ar980030v CCC: $18.00
Published on Web 01/14/1999

between the metal and the organic material.[22,23] This model considers charge distribution at and near the metal/organic interface based on the relative energy levels of the metal Fermi energy and the energy of formation of excited states such as polarons and bipolarons. Brazovskii and Kirova considered a thermodynamic model to investigate the interface between a metal and a conjugated polymer.[22] By requiring thermal equilibrium and realizing easy deformation of polymer chains, they found that the charge transfer from the metal to the polymer was stabilized by the formation of a soliton or bipolaron lattice in the polymer near the interface region, resulting in a built-in electric field of about 10^7-10^8 V/m. The Fermi level of the metal always lies inside the energy gap, and the sign of the carriers is determined by the work function difference between the metal and the polymer. The thermodynamic model of polymer LEDs reported by Davids et al. refines the work of Brazovskii and Kirova by specifically considering charge carriers.[23] The free energy density F has the form[23]

$$F = \sum_i (E_i - (\mu_0 + e\phi)\delta_i)n_i - kT\ln(\Omega)/V - \frac{\epsilon}{8\pi}\left(\frac{\mathrm{d}\phi}{\mathrm{d}x}\right)^2 \quad (1)$$

where i labels the various charged excitations and traps, E_i is the energy of the excitation or trap, μ_0 is the chemical potential of the metal contact, e is the magnitude of the electron charge, ϕ is the electrostatic potential, δ_i is the charge of the excitation or trap in units of e, n_i is the density function for the excitation or trap, T is the temperature, ϵ is the low-frequency dielectric constant of the polymer, and x is the position. The entropy density is given by

$$S = k\ln(\Omega)/V \quad (2)$$

where k is Boltzmann's constant and Ω is the number of configurations for the charge excitations and traps in the volume V. The thermodynamic model predicts charge transfer and band bending at the metal/polymer interface due to the formation of polarons/bibolarons or traps.

2.2. Quantum Mechanical Model. The quantum mechanical model of the metal/organic interface is based on quantum chemistry calculations to understand the molecular properties of the interfaces.[24−29] In this case, the interaction between metal atoms and the polymer is inferred from quantum mechanical calculations which attempt to minimize the energy of the system. This approach offers the advantage of considering the interaction between the metal atoms and specific functionality of the organic material. Even in the case of relatively small molecules, Schrödinger's equation cannot be solved exactly, and various approximations have been devised to address this issue. The Hamiltonian which describes a system consisting of many interacting bodies contains several terms to describe the various interactions. Using the Born−Oppenheimer approximation, the electronic part of the Hamiltonian H^e can now be separated and yields

$$\hat{H}^{\mathrm{e}} = -\frac{\hbar^2}{2m_{\mathrm{e}}}\sum_{i=1}^{N_{\mathrm{e}}}\hat{\nabla^2} - e^2\sum_{A=1}^{N_{\mathrm{n}}}\sum_{i=1}^{N_{\mathrm{e}}}\frac{Z_{\mathrm{A}}}{|R_{\mathrm{A}} - r_i|} + \frac{e^2}{2}\sum_{i=1}^{N_{\mathrm{e}}}\sum_{j\neq 1}\frac{1}{|r_i - r_j|} \quad (3)$$

where r_i and R_A are the position vectors of the electrons and nuclei, respectively, Z_A is the charge of the nuclei, and N_{n} and N_{e} are the numbers of nuclei and electrons, respectively. The first term designates the kinetic energy of the electrons, the second is the potential energy of the electrons that results from the attraction to the nuclei, and the third term represents the repulsion of the electrons. Next, the electrons are taken to interact with the field obtained by averaging over the positions of the remaining electrons, as prescribed by the Hartree−Fock (H−F) approximation.

On the basis of such calculations, it has been postulated that the metal employed plays an important role in determining the extent of charge transfer that occurs. For example, Dannetun et al. found that aluminum appears to bond covalently to PPV, with the vinylene groups being the preferred site.[25] Al therefore disrupts the chemical structure of the surface of the conjugated polymer sample. In the case of sodium, charge transfer from the metal to the polymer gives rise to two new in-gap states at the interface without significantly altering its chemistry.[26] It was found that the local spin density (LSD)[28] method provides good estimates of the positions of the gap states while the valence effective Hamiltonian pseudopotential (VEH)[29] method tends to overestimate the splitting of these states for small systems.

The theoretical understanding of the interface formation in OLEDs is still evolving, and different models have been presented. Taken together, these models offer insight into the processes that occur during the interface formation, as well as its implications for charge injection and transport across the interface.[8,9,30−32]

3. Investigations Using Surface and Interface Analytical Techniques

Surface/interface analytical techniques have proven powerful in studying inorganic semiconductors[33] as well as organic semiconductor devices.[34] Among many of these techniques, X-ray photoemission spectroscopy (XPS),[35] ultraviolet photoemission spectroscopy (UPS),[35] near edge X-ray absorption fine structure (NEXAFS),[36] scanning tunneling microscopy (STM),[37] and atomic force microscopy (AFM)[38] have been the most successfully applied to study interface formation in OLEDs. In the following sections, examples are presented to demonstrate the up-to-date microscopic understanding of the electronic, chemical, and morphology structures of the interfaces achieved by means of surface and interface analytical techniques.

3.1. Interface Interaction and Level Bending. The interface reaction between the metal and organic may be characterized by charge transfer and chemical reaction,

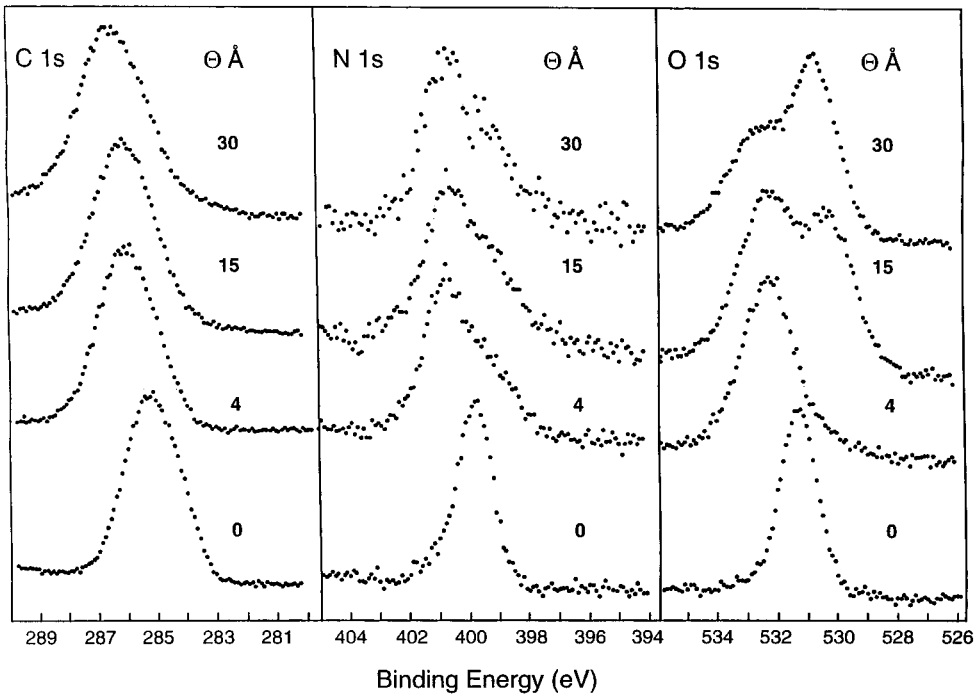

FIGURE 1. Evolution of XPS C 1s, O 1s, and N 1s core level EDCs as a function of increasing Ca thickness Θ_{Ca} on Alq_3. Reprinted with permission from ref 39. Copyright 1998 American Institute of Physics.

and for a given system both may exist. Choong et al. found a staged interface formation initialized by charge transfer and then chemical reaction for Ca on tris(8-hydroxyquinoline)aluminum (Alq_3), a prototypical molecular EL material.[39] Shown in Figure 1 is the evolution of XPS C 1s, O 1s, and N 1s core level electron density curves (EDCs) as a function of increasing Ca thickness Θ_{Ca} on Alq_3. At $\Theta_{Ca} = 0$ Å, these core level EDCs are Gaussian in shape and composed of only one component, indicating a clean Alq_3 film. As early as $\Theta_{Ca} = 1$ Å, the emergence of a new component is observed in the N 1s EDCs. The O 1s EDCs remain single component until $\Theta_{Ca} = 4$ Å, indicating that the phenoxide side of the ligand is relatively unaffected by the presence of Ca. As more Ca is deposited, the O 1s EDC splits, and a new reacted component occurs at lower binding energy, which increases in intensity and shifts back to higher binding energy with increasing coverage. The intensity and position of the reacted N 1s component remain almost constant with coverage above about 4 Å. Clearly Ca interacts with N first, and once the Ca−N interaction is saturated, Ca−O reaction takes place. The interaction between Ca and N is a charge-transfer process yielding a stable Alq_3 radical anion and Ca^{2+}, a fact supported by the binding energy of Ca 2p for $\Theta_{Ca} \leq 4$ Å. The precise picture of the interface reaction can be obtained by decomposition of the O 1s and N 1s EDCs. Shown in Figure 2 are representative decompositions for N 1s (Figure 2a) and O 1s (Figure 2b). From the decomposition, it is clear that the binding energies (BEs) of the new N and O components are approximately 1.7 and 2.0 eV lower than those of the unreacted components, indicating that the reaction is not due to morphological inhomogeneity. Also, the 1:2 ratio of reacted and nonreacted components of N 1s can be observed, reaffirming

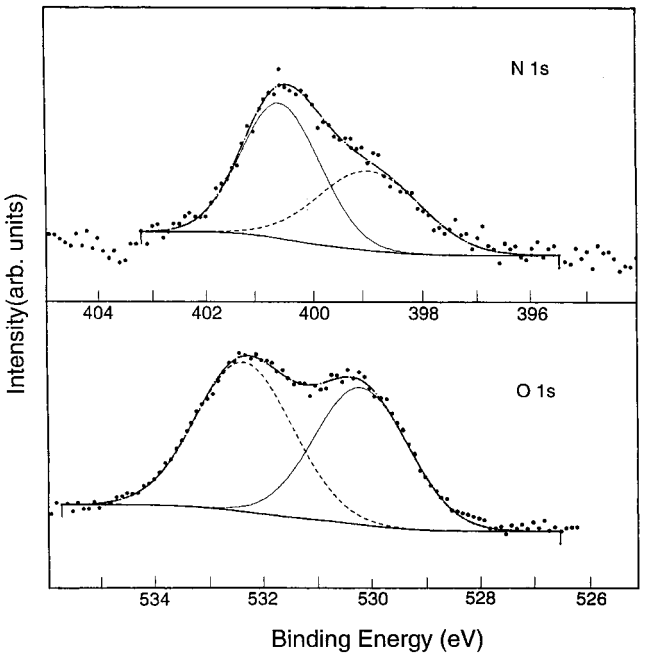

FIGURE 2. Decomposition of representative XPS (a) O 1s and (b) N 1s EDCs. Reprinted with permission from ref 39. Copyright 1998 American Institute of Physics.

that one of the three quinolates of Alq_3 accepts the electron donated by Ca before the resulting structural deformation of the Alq_3 allows the chemical reaction between Ca and O.

The interface level bending in the organic material is exemplified at the interface of Ca and a model phenylenevinylene oligomer, 4,4′-bis[4-(3,5-di-*tert*-butylstyryl)-styryl]stilbene (5PV), as observed by Park et al.[40] The evolution of C 1s peaks with increasing 5PV coverage Θ_{5PV} is shown in Figure 3. The inset shows the chemical

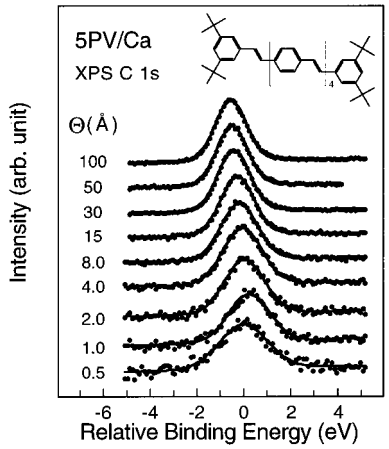

FIGURE 3. Evolution of XPS C 1s peaks as a function of 5PV layer thickness Θ_{PV} on Ca substrate. The movement of the peak position toward the lower BE is obvious. The inset shows the structure of 5PV. Reprinted with permission from ref 40. Copyright 1996 American Institute of Physics.

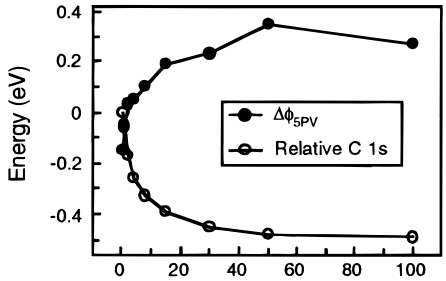

FIGURE 4. Relative position of the C 1s peak and the difference between the work function of Ca and 5PV ($\Delta\phi_{5PV} = \phi_{5PV} - \phi_{Ca}$) with increasing Θ. Adjusted for a constant offset, the two curves are essentially mirror images of each other. Reprinted with permission from ref 40. Copyright 1996 American Institute of Physics.

structure of 5PV. There is a gradual peak movement toward lower binding energy. The peak is broader below $\Theta_{5PV} = 15$ Å and becomes identical to that for the bulk 5PV at $\Theta_{5PV} \geq 30$ Å. The data are fitted with a single Gaussian as shown by solid lines. The broader peaks at lower coverage may be due to excess charges that are transferred from the Ca substrate to the submonolayer of 5PV. The excess charges can be inhomogeneously distributed within a molecule. It has been reported that the Ca atoms deposited on PPV interact preferentially with carbon atoms in the vinylene chains by charge transfer.[41] This may happen at the initial 5PV deposition on Ca and result in the observed peak broadening.

The relative positions of the C 1s peak as a function of Θ_{5PV} are shown in Figure 4 after correction with respect to substrate Ca 2p position. It also shows the change in work function $\Delta\phi_{5PV} = \phi_{5PV} - \phi_{Ca}$. It is obvious that these two curves are essentially mirror images with a constant offset. The total change (~0.5 eV) is the same for each curve. This is strong evidence that the charge transfer during interface formation results in a shift in binding energy in a manner similar to band bending. It is also clear that the level bending extends up to about 100 Å inside the 5PV layer. The offset of the vacuum level at the interface is a general phenomenon. The 5PV/Ca interface

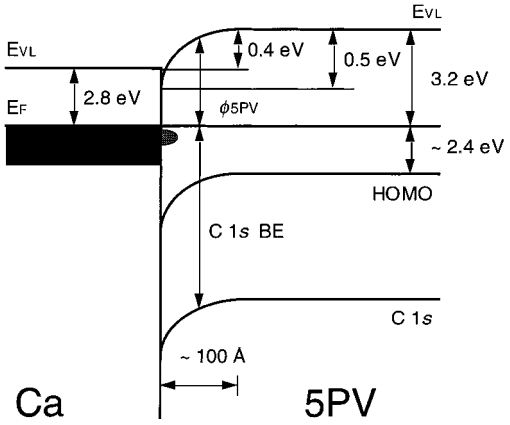

FIGURE 5. Energy level diagram for the 5PV/Ca interface constructed from data obtained by XPS and UPS. Positions of relevant levels relative to the Fermi level are indicated except for the LUMO level. The interface gap states are schematically shown.

can be described as having a weak dipole layer and a carrier concentration to allow for a 100 Å thick space charge layer. An energy level diagram deduced from the above observations is illustrated in Figure 5. An interesting feature shown in Figure 5 is the offset of the vacuum level E_{VL} at the interface, which demonstrates the invalidity of the assumption that there exists a common vacuum level in OLED. The interface gap states are schematically shown in Figure 5. These interface states can form from charge transfer, wave function hybridation, and chemical reactions. For example, the formation of bipolaron states for Ca on poly(2,5-diheptyl-*p*-phenylenevinylene) has been reported from UPS studies.[24]

The fundamental difference between the interface level bending in organic and inorganic semiconductors is that, in an organic material, the interface level bending is localized to within a few monolayers from the metal surface, and it results from charge transfer, dipole alignment, and chemical reactions in the vicinity of the metal surface. In contrast, in an inorganic semiconductor band bending is over a much extended region, facilitated by either depletion or accumulation of the majority carriers doped in the semiconductor.

3.2. Near Edge X-ray Absorption Fine Structure Studies. NEXAFS is a unique technique that directly probes the evolution of unoccupied states with elemental selectivity.[36] In the NEXAFS study by Ettedgui et al. on the interface formation between metals and conjugated polymers, the first direct evidence for differences in the evolution of unoccupied states induced by the deposition of Ca and Al on poly(2,3-(diphenylphenyl)vinylene) (DP−PPV) was observed.[42] Shown in Figure 6 is the evolution of the C_K-edge NEXAFS spectrum of DP−PPV during the course of Al deposition.[42] The spectrum of clean DP−PPV reflects contributions primarily from the phenylene portion of the molecules, and the features near 287, ~290, and 293−315 eV are attributed to the π_1* and π_2* structures, and the σ_1* and σ_2* regions, respectively. A detailed comparison of the NEXAFS spectra obtained for clean DP−PPV as well as after the deposition of 30 Å Al shows

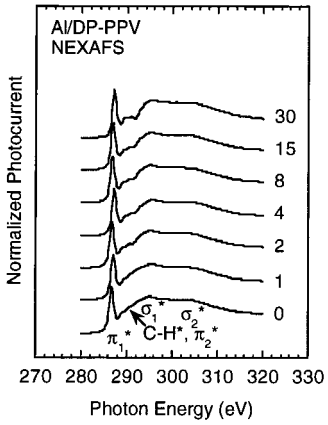

FIGURE 6. Evolution of the NEXAFS spectrum during the deposition of Al on DP−PPV. The labeled features correspond to transitions of the C 1s core-level electron to unoccupied states. The spectra change little as the Al layer increases to 30 Å. Reprinted with permission from ref 42. Copyright 1996 American Institute of Physics.

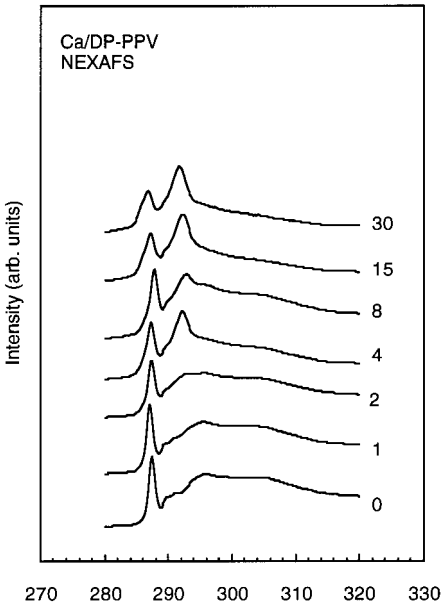

FIGURE 7. Evolution of the NEXAFS spectrum during the deposition of Ca on DP−PPV. The changes after >4 Å Ca reflect charge transfer across the metal/polymer interface. Reprinted with permission from ref 42. Copyright 1996 American Institute of Physics.

a loss in signal intensity within the C−H* and π_2* regions due to Al deposition.

The evolution in the NEXAFS spectra following the deposition of Ca differs markedly from those observed for Al. Figure 7 shows the evolution of the NEXAFS spectrum of DP−PPV during the course of Ca deposition.[42] Following the deposition of 30 Å Ca, an increase within the leading edge of the π_1* resonance is found in the photocurrent compared to that of the clean sample, indicating the formation of new intragap states. The changes in the unoccupied states of DP−PPV following the deposition of Ca may result from charge transfer across the Ca/DP−PPV interface. The creation of these additional unoccupied states at the Ca/DP−PPV interface may enhance charge injection for EL by providing additional sites for electron transfer into the polymer near the Fermi level of the metal.

3.3. Scanning Tunneling Microscopy Investigations. Scanning tunneling microscopy is one of the best tools capable of providing an image of a materials surface on a nanometer scale.[37] It can provide high-resolution images of molecular adsorbates and atoms on the surface. Because of these capabilities, STM has been used on a wide range of subjects in physics, materials science, chemistry and biology. STM was used by Razafitrimo et al. to provide insight into the geometrical structure at the interface in an OLED.[43] By investigating every surface of a three-layer device, one at a time, the profile of the interfaces in the device can be drawn.[43]

The topographies of the Ag top electrode (a), the spin cast polymer (b), and the ITO coated glass substrate (c) are presented in Figure 8. The size of the pictures is 5200 Å × 5200 Å, and a corner of every image was magnified by 10. The ITO coating shows a granular structure with some larger ITO flakes, but small grains are the dominating feature, as shown by the magnification on the upper right of the image. The ITO coating does not show any particular orientation. In contrast, the polymer presents large coalescing bundles, containing a fibrous-like structure, as shown in Figure 8b. The fibers of molecules extend in a direction perpendicular to the radial force from the spin casting. The bundle-like structure of the polymer is homogeneous over all areas. The 400 Å thick polymer smears out completely the ITO structure. The top Ag layer shows the typical cluster-like structure of vacuum deposited Ag. The graphical enhancement at the upper right of Figure 8a helps to distinguish the large Ag clusters. Atomic force microscopy images of Ag evaporated on the polymer film are similar to those of Ag one evaporated onto the bare ITO substrate. STM and AFM have also been applied to study polymer films prepared by different methods and on different substrates.[43,44] These studies reveal nanometer scale structures in polymeric LEDs caused by the substrate, the polymer film, and the top electrode, which may significantly alter the local electric field and therefore profoundly affect the performance and lifetime of polymeric LEDs.

3.4. Quenching of Luminescence of Organic Materials by Metal Electrodes. At a metal/organic interface, charge transfer from the metal to the organic materials may induce gap states associated with lattice deformation of the organic material,[22,23] as discussed in section 2.3. These states may also form quenching centers to the luminescence of organic materials.[45−48] Shown in Figure 9 is the photoluminescence (PL) intensity plotted as a function of Θ_{Ca} for a 300 Å 4PV film, observed by Choong et al.[45] The rate of intensity decrease can be divided into three stages. The first stage is between $\Theta_{Ca} = 0$ Å and $\Theta_{Ca} = 1$ Å, the second between $\Theta_{Ca} = 1$ Å and $\Theta_{Ca} = 30$ Å, and the third for $\Theta_{Ca} > 30$ Å. The first stage accounts for the reduction of the PL intensity by 65% and is due to the fact that the Ca atoms provide nonradiative decay channels. After the initial drop, the effect of PL quenching by Ca atoms is reduced, as indicated by a slower rate of PL quenching observed in the second stage, as the quenching region of additional Ca atoms overlaps with existing ones.

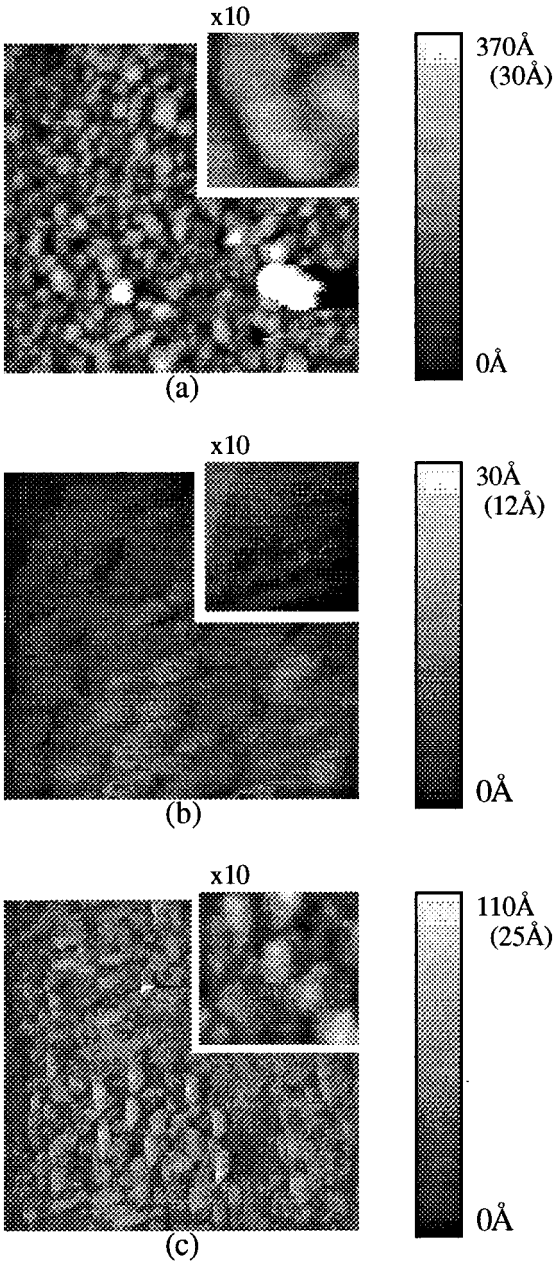

FIGURE 8. Images of different layers relevant to LED: (a) 100 Å Ag electrode on DP−PPV/ITO, (b) 400 Å DP−PPV on ITO, and (c) ITO substrate. Window sizes are 5000 Å × 5000 Å and 500 Å × 500 Å in every inset.

In the third stage, $\Theta_{Ca} > 30$ Å, the drop in PL intensity is due solely to the attenuation of both excitation and emission photons due to the thickness of the Ca layer as it becomes metallic.[45]

Park et al. found that the PL quenching due to Ca deposition can be recovered after exposure to oxygen.[46] The crucial role of the oxidized Ca layer is clearer when the PL intensity evolutions of Ca/4PV with and without the oxidation process are compared, as shown in Figure 10. The bottom curve of Figure 10b is the PL intensity as a function of Ca thickness without the oxidation process. Here a monotonic intensity decrease is evident. The middle curve is the PL intensity after each fresh deposition of Ca on previously oxidized Ca/4PV. For example, the

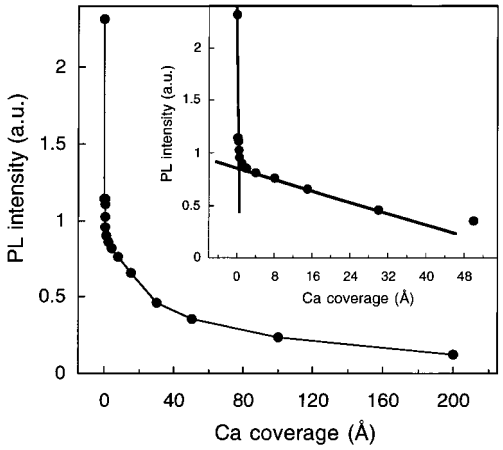

FIGURE 9. Evolution of PL peak intensity as a function of Ca coverage, Θ_{Ca}. Three distinct stages of PL intensity decrease are observed. Reprinted with permission from ref 45. Copyright 1996 American Institute of Physics.

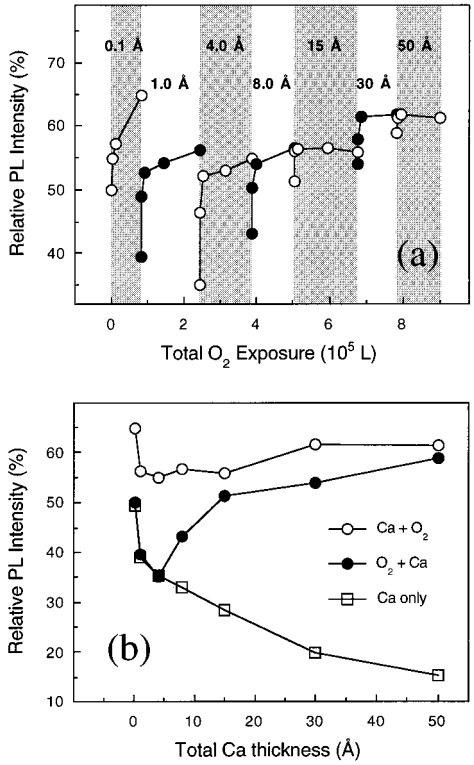

FIGURE 10. (a) PL intensity under a sequence of Ca deposition and oxidation cycles. (b) PL intensity taken with respect to Ca thickness under three different conditions. Reprinted with permission from ref 46. Copyright 1997 American Institute of Physics.

data point at 8 Å is the PL intensity after 4 Å of fresh Ca was deposited on the 4 Å oxidized Ca/4PV layer. The middle curve shows how effective a given calcium oxide layer is in protecting 4PV PL from fresh Ca. The top curve in Figure 10b shows the PL intensity at the end of the oxidation process at a given Ca thickness. The PL intensity of oxidized Ca/4PV remains between 55 and 65% of that of pristine 4PV up to 50 Å of oxidized Ca layer. On the other hand, the PL from unoxidized Ca decreases to around 15% after deposition of 50 Å of Ca. These numbers suggest that a proper oxidation of Ca at the Ca/4PV

interface could significantly improve the efficiency of a single layer EL device.

The quenching phenomenon is quite common, as observed by Choong et al. for Ca, Al, and Ag on 4PV,[47] and Ca, Ag, and Ge on Alq_3.[48] It has the most severe adverse effect on single layer devices based on hole conducting materials, such as PPV and its derivatives, because the radiative recombination zone in these devices is close to the metal cathode. For electron conducting materials, the problem will be much less significant since the recombination zone is close to the ITO anode, on which no quenching of PL is observed.[47] It is also less important for multilayer devices with both electron conducting and hole conducting layers, since the emission zone will be localized at the organic/organic interface,[1] provided that the electron conducting layer is substantially thicker than the combination of exciton diffusion length and cathode metal penetration depth.

3.5. Other Examples of Surface Analytical Work. The above is not intended to be an exhaustive review of all the possible uses of these surface analytical tools for investigations of organic semiconductor devices. Certainly, there are many other examples that illustrate the application of surface techniques to interface formation of OLEDs. Further insight can be obtained by observing the fine structure of the core levels. Dannetun et al. observed the shake-up spectra of the C 1s core level for Al/PPV, and the gradual reduction of the shake-up feature following Al deposition is interpreted as evidence of Al preferential interaction with the vinylene groups.[49] Johansson et al. observed the chemistry at the interface between PPV and ITO deposited by argon sputtering, and found different oxidized states of PPV due to the sputtering.[50] Nguyen et al. studied the interface formation of a number of metals with PPV using XPS and attenuated total reflection infrared spectroscopies, and suggested the formation of metal carbide in the polymer.[51] Seki et al.[52] and Rajagopal et al.[53] investigated the energy level alignment at a number of organic/metal and organic/organic interfaces using UPS, and confirmed the invalidity of the traditional model for energy level alignment with respect to a common vacuum level. Probst and Haight investigated the temporal evolution of Ga and Ca vacuum deposited onto thin films of Alq_3 and found that Ga diffused into the organic at room temperature while Ca did not.[54] It is clear that more surface analytical tools that probe the electronic and atomic structure of materials will be applied to study the phenomena in the future, and a more complete picture of the interface formation in organic semiconductor devices can be expected to emerge as a result.

4. Final Remarks

Despite the strong dependence of the device performance on interfaces, the detailed properties and roles of interfaces in the OLED devices remain to be fully characterized. The mismatch between a strong metallic lattice and a weak van der Waals organic solid at the metal/organic interface could result in an interfacial structure which is uniquely different from those commonly found in metal/inorganic semiconductors. Thus, the fundamental issues regarding metal/organic interfaces, such as the formation of the Schottky type barrier, the diffusiveness of the interface, and the origin of ionized species, are critical for further advancement of OLEDs and merit systematic investigations. Likewise, the organic/organic interfaces between molecules of dissimilar charge transport properties are important in high-efficiency bilayer OLEDs. Surface and interface analytical investigations of the interfaces in OLEDs have generated critical insight into the fundamental processes at these interfaces. These studies have shown that the design and control of surfaces and interfaces are likely to be the areas with the highest return on investment in terms of delivering stable organic devices.

This work was supported in part by the NSF (Grant DMR-9612370) and by DARPA (Grant DAAL-0196K0086). I gratefully acknowledge the efforts of a group of talented individuals responsible for the studies summarized herein: Emile Ettedgui, Haja Razafitrimo, Vi-En Choong, and Yongsup Park. I also acknowledge Drs. Gary Mason and Ching Tang of Eastman Kodak for a fruitful collaboration.

References

(1) Tang, C. W.; VanSlyke, S. A. Organic Electroluminescent Diodes. *Appl. Phys. Lett.* **1987**, *51*, 913.
(2) Burroughes, J. H.; Bradley, D. D. C.; Brown, A. R.; Marks, R. N.; MaKay, K.; Friend, R. H.; Burn, P. L.; Holmes, A. B. Light-Emitting-Diodes Based on Conjugated Polymers. *Nature* **1990**, *347*, 539.
(3) Gustafsson, G.; Cao, Y.; Treacy, G. M.; Klavetter, F.; Colaneri, N.; Heeger, A. J. Flexible Light-Emitting Diodes Made from Soluble Conducting Polymers. *Nature* **1992**, *357*, 477.
(4) Forrest, S. R.; Burrows, P. E.; Shen, Z.; Gu, G.; Bulovic, V.; Thompson, M. E. The Stacked OLED (SOLED): a New Type of Organic Device for Achieving High-Resolution Full-Color Displays. *Synth. Met.* **1997**, *91*, 9.
(5) Tessler, N.; Denton, G. J.; Friend, R. H. Lasing Characteristics of PPV Microcavities. *Nature* **1996**, *382*, 695.
(6) Braun, D.; Heeger, A. J. Visible-Light Emission from Semiconducting Polymer Diodes. *Appl. Phys. Lett.* **1991**, *58*, 1982.
(7) Brown, A. R.; Bradley, D. D. C.; Burroughes, J. H.; Friend, R. H.; Greenham, N. C.; Burn, P. L.; Holmes, A. B.; Kraft, A. Poly(*p*-phenylenevinylene) Light-Emitting-Diodes − Enhanced Electroluminescency through Charge Carrier Confinement. *Appl. Phys. Lett.* **1992**, *61*, 2793.
(8) Parker, I. D. Carrier Tunneling and Device Characteristics in Polymer Light-Emitting Diodes. *J. Appl. Phys.* **1994**, *75*, 1656.
(9) Yang, Y.; Heeger, A. J. A New Architecture for Polymer Transistors. *Nature* **1994**, *372*, 344.
(10) Bröms, P.; Birgersson, J.; Johansson, N.; Lögdlund, M.; Salaneck, W. R. Calcium Electrodes in Polymer LEDs. *Synth. Met.* **1995**, *74*, 179.
(11) Kim, Y.-E.; Park, H.; Kim, J.-J. Enhanced Quantum Efficiency in Polymer Electroluminescence Devices by Inserting a Tunneling Barrier Formed by Langmuir−Blodgett Films. *Appl. Phys. Lett.* **1996**, *69*, 599.

(12) Hung, L. S.; Tang, C. W.; Mason, M. G. Enhanced Electron Injection in Organic Electroluminescence Devices Using an Al/LiF Electrode. *Appl. Phys. Lett.* **1997**, *70*, 152.
(13) Jabbour, G. E.; Kawabe, Y.; Shaheen, S. E.; Wang, J. F.; Morrell, M. M.; Kippelen, B.; Peyghambarian, N. Highly Efficient and Bright Organic Electroluminescent Devices with an Auminum Dathode. *Appl. Phys. Lett.* **1997**, *71*, 1762.
(14) Tang, H.; Li, F.; Shinar, J. Bright High Efficiency Blue Organic Light-Emitting Diodes with Al2O3/Al Cathodes. *Appl. Phys. Lett.* **1997**, *71*, 2560.
(15) Haskal, E. I.; Curioni, A.; Seidler, P. F.; Andreoni, W. Lithium−Aluminum Contacts for Organic Light-Emitting Devices. *Appl. Phys. Lett.* **1997**, *71*, 1151.
(16) Gyoutoku, A.; Hara, S.; Komatsu, T.; Shirinashihama, M.; Iwanaga, H.; Sakanoue, K. An Organic Electroluminescent Dot-Matrix Display Using Carbon Underlayer. *Synth. Met.* **1997**, *91*, 73.
(17) Nuesch, F.; SiAhmed, L.; Francois, B.; Zuppiroli, L. Derivatized Electrodes in the Construction of Organic Light Emitting Diodes. *Adv. Mater.* **1997**, *9*, 222.
(18) Wu, C. C.; Wu, C. I.; Sturm, J. C.; Kahn, A. Surface Modification of Indium Tin Oxide by Plasma Treatment: An Effective Method to Improve the Efficiency, Brightness, and Reliability of Organic light emitting devices. *Appl. Phys. Lett.* **1997**, *70*, 1348.
(19) Service, R. F. Your (Light-Emitting) Logo Here. *Science* **1998**, *279*, 1135.
(20) Antoniadis, H.; Hueschen, M. R.; Miller, J. N.; Moon, R. L.; Roitman, D. B.; Sheats, J.R. Failure Modes in Vapor-Deposited Organic LED's. *Macromol. Symp.* **1998**, *125*, 59.
(21) Heeger, A. J.; Kivelson, S.; Schrieffer, J. R.; Su, W.-P. Solitons in Conducting Polymers. *Rev. Mod. Phys.* **1988**, *60*, 781.
(22) Brazovskii, S. A.; Kirova, N. N. Towards the Theory of Metal−Polymer Contact. *Synth. Met.* **1993**, *55*−*57*, 4385.
(23) Davids, P. S.; Saxena, A.; Smith, D. L. Nondegenerate Continuum Model for Polymer Light-Emitting-Diodes. *J. Appl. Phys.* **1995**, *78*, 4244.
(24) Salaneck, W. R.; Stafstroem, S.; Bredas, J. L. *Conjugated Polymer Surfaces and Interfaces*; Cambridge: New York, 1996.
(25) Dannetun, P.; Löglund, M.; Fahlman, M.; Boman, M.; Stafström, S.; Salaneck, W. R.; Lazzaroni, R.; Fredriksson, C.; Brédas, J. L.; Graham, S.; Friend, R. H.; Holmes, A. B.; Zamboni, R.; Taliani, C. The Chemical and Electronic Structure of the Interface between Aluminum and Conjugated Polymers or Molecules. *Synth. Met.* **1993**, *55*, 212.
(26) Löglund, M.; Dannetun, P.; Fredriksson, C.; Salaneck, W. R.; Brédas, J. L. Theoretical Study of the Interaction between Sodium and Oligomers of Poly(*p*-phenylenevinylene) and Poly(*p*-phenylene). *Synth. Met.* **1994**, *67*, 141.
(27) Choong, V.; Park, Y.; Gao, Y.; Hsieh, B. R. Quantum Molecular Quantum Mechanical Calculations of the Interface Formation between Al, Ca and Mg with Poly(Phenylene Vinylene) (PPV) Oligomers. *J. Phys.* **1997**, *D30*, 1421.
(28) Vosko, S. H.; Wilk, L.; Nusair, M. Accurate Spin-Dependent Electron Liquid Correlation Energies for Local Spin Density Calculations: a Critical Review. *Can. J. Phys.* **1980**, *58*, 1200.
(29) Salaneck, W. R.; Brédas, J. L. Electronic and Chemical Structure of Conjugated Polymers and Their Interfaces − Experiment, Theory and a Glance toward the Future. *Synth. Met.* **1994**, *67*, 11.
(30) Ettedgui, E.; Razafitrimo, H.; Gao, Y.; Hsieh, B. R. Band Bending Modified Tunneling at Metal/Conjugated Polymer Interfaces. *Appl. Phys. Lett.* **1995**, *67*, 2705.
(31) Davids, P. S.; Campbell, I. H.; Smith, D. L. Device Model for Single Carrier Organic Diodes. *J. Appl. Phys.* **1997**, *82*, 6319.
(32) Conwell, E. M.; Wu, M. W. Contact Injection into Polymer Light-Emitting Diodes. *Appl. Phys. Lett.* **1997**, *70*, 1867.
(33) Brillson, L. J. In *Handbook on Semiconductors*; Landsberg, P. T., Ed.; Elsevier Science Publishers: New York, 1992; Vol. 1.
(34) Löglund, M.; Dannetun, P.; Salaneck, W. R. *Handbook of Conducting Polymers*; in press.
(35) *Methods of Experimental Physics*; Park, R. L., Lagally, M. G., Eds; Academic Press: Orlando, 1985; Vol. 22.
(36) Stöhr, J. *NEXAFS Spectroscopy*; Springer Series in Surface Sciences 25; Springer-Verlag: New York, 1992.
(37) Binnig, G.; Rohrer, H. R. Scanning Tunneling Microscopy. *Helv. Phys. Acta* **1982**, *55*, 726.
(38) Binnig, G.; Quate, C. F.; Gerber, C. Atomic Force Microscope. *Phys. Rev. Lett.* **1986**, *56*, 930.
(39) Choong, V. E.; Mason, M. G.; Tang, C. W.; Gao, Y. Investigation of the Interface Formation Between Calcium and Tris-(8-hydroxy quinoline) aluminum. *Appl. Phys. Lett.* **1998**, *72*, 2689.
(40) Park, Y.; Ettedgui, E.; Choong, V.; Gao, Y.; Hsieh, B. R.; Wehrmeister, T.; Mullen, K. Energy Level Bending and Alignment at the Interface between Ca and a Phenylene Vinylene Oligomer. *Appl. Phys. Lett.* **1996**, *69*, 1080.
(41) Salaneck, W. R.; Brédas, J. L. The Metal-on-Polymer Interface in Polymer Light Emitting Diodes. *Adv. Mater.* **1996**, *8*, 48.
(42) Ettedgui, E.; Razafitrimo, H.; Gao, Y.; Hsieh, B. R.; Feld, W. A.; Ruckman, M. W. Evidence for the Formation of Unoccupied States in Poly(2,3-diphenyl phenylene vinylene) Following the Deposition of Metal. *Phys. Rev. Lett.* **1996**, *76*, 299.
(43) Razafitrimo, H.; Gao, Y.; Hsieh, B. R. A Layer-wise Topographic Study of a Polymeric Light Emitting Diode: Indium Tin Oxide/Poly(diphenyl phenylene vinylene)/Ag. *Synth. Met.* **1996**, *79*, 103.
(44) Rasmusson, J. R.; Broms, P.; Birgerson, J.; Erlandsson, R.; Salaneck, W. R. The Interface Surfaces of a CN-substituted Poly(phenylenevinylene) Light-Emitting Diode, a Morphological Study. *Synth. Met.* **1996**, *79*, 75.
(45) Choong, V.; Park, Y.; Gao, Y.; Wehrmeister, T.; Müllen, K.; Hsieh, B. R.; Tang, C. W. Dramatic Photoluminescence Quenching of Phenylene Vinylene Oligomer Thin Films upon Submonolayer Ca Deposition. *Appl. Phys. Lett.* **1996**, *69*, 1492.
(46) Park, Y.; Choong, V.; Hsieh, B. R.; Tang, C. W.; Gao, Y. Gap-State Induced Photoluminescence Quenching of Phenylene Vinylene Oligomer and its Recovery by Oxidation. *Phys. Rev. Lett.* **1997**, *78*, 3955.
(47) Choong, V.; Park, Y.; Hsieh, B. R.; Tang, C. W.; Wehrmeister, T.; Müllen, K.; Gao, Y. Effects of Metals on Luminescence of Organic Materials. *J. Vac. Sci. Technol.* **1997**, *A15*, 1745.
(48) Choong, V.; Park, Y.; Shivaparan, N.; Tang, C. W.; Gao, Y. Deposition Induced Photoluminescence Quenching of Tris-(8-Hydroxyquinoline) Aluminum. *Appl. Phys. Lett.* **1997**, *71*, 1005.
(49) Logdlund, M.; Salaneck, W. R.; Meyers, F.; Bredas, J. L.; Arbuckle, G. A.; Friend, R. H.; Holmes, A. B.; Froyer, G. Evolution of the Electronic Structure in a Conjugated Polymer Series − Polyacetylene, Poly-

(*p*-phenylene), and Poly(*p*-phenylenevinylene). *Macromolecules* **1993**, *26*, 3815.
(50) Johansson, N.; Cacialli, F.; Xing, K. Z.; Beamson, G.; Clark, D. T.; Friend, R. H.; Salaneck, W. R. A Study of the ITO-on-PPV Interface Using Photoelectron Spectroscopy. *Synth. Met.* **1998**, *92*, 207.
(51) Nguyen, T. P.; Massardier, V.; Tran, V. H.; Guyot, A. Studies of the Polymer−Metal Interface in Metal-PPV-Metal Devices. *Synth. Met.* **1993**, *55*−*57*, 235.
(52) Seki, K.; Ito, E.; Ishii, H. Energy Level Alignment at Organic/metal Interfaces Studied by UV Photoemission. *Synth. Met.* **1997**, *91*, 137.
(53) Rajagopal, A.; Kahn, A. Molecular-Level Offset at the PTCDA/Alq(3) Heterojunction. *Adv. Mater.* **1998**, *10*, 140.
(54) Probst, M.; Haight, R. Unoccupied Molecular Orbital States of Tris (8-hydroxy quinoline) aluminum: Observation and Dynamics. *Appl. Phys. Lett.* **1997**, *70*, 1420.

AR980030V